Title
Alternative definitions of the frozen energy in energy decomposition analysis of density functional theory calculations

Journal
The Journal of Chemical Physics, 144(8)

ISSN
0021-9606

Authors
Horn, Paul R
Head-Gordon, Martin

Publication Date
2016-02-28

DOI
10.1063/1.4941849

Peer reviewed

Alternative definitions of the frozen energy in energy decomposition analysis of density functional theory calculations

Paul R. Horn[1, a)] and Martin Head-Gordon[1, b)]
Kenneth S. Pitzer Center for Theoretical Chemistry, Department of Chemistry, University of California, Berkeley, CA 94720 and Chemical Sciences Division Lawrence Berkeley National Laboratory Berkeley, CA, 94720 Phone: 510-642-5957 Fax: 510-643-1255

In energy decomposition analysis (EDA) of intermolecular interactions calculated via density functional theory, the initial supersystem wavefunction defines the so-called "frozen energy" including contributions such as permanent electrostatics, steric repulsions and dispersion. This work explores the consequences of the choices that must be made to define the frozen energy. The critical choice is whether the energy should be minimized subject to the constraint of fixed density. Numerical results for Ne_2, $(H_2O)_2$, BH_3-NH_3, and ethane dissociation show that there can be a large energy lowering associated with constant density orbital relaxation. By far the most important contribution is constant density inter-fragment relaxation, corresponding to charge transfer (CT). This is unwanted in an EDA that attempts to separate CT effects, but it may be useful in other contexts such as force field development. An algorithm is presented for minimizing single determinant energies at constant density both with and without CT by employing a penalty function that approximately enforces the density constraint.

I. INTRODUCTION

In electronic structure theory, an energy decomposition analysis (EDA) is a partition of the interaction energy of a system of fragments, an observable, into a sum of energy terms that are not observables but carry chemical meaning[1–5]. Such terms typically include polarization, charge transfer (CT), permanent electrostatics, dispersion, and Pauli repulsion. These decompositions are not uniquely defined but can be useful in building intuition about a given system. Because the total energy of interest is the difference between that of the supersystem and the non-interacting component subsystems, the decompositions generally involve a progression from many subsystem wavefunctions to a single, optimal supersystem wavefunction.

The focus of this paper is the first intermediate electronic wavefunction in this sequence which treats all electrons in the system together. The associated energy is usually called the "frozen energy" and its meaning relative to the energies of the isolated subsystems is usually taken as a combination of permanent electrostatics and Pauli repulsion.[4] The construction of the initial supersystem wavefunction for the single Slater determinant case of Kohn-Sham density functional theory (DFT) or Hartree-Fock (HF) theory is the central concern of this work. A single Slater determinant wavefunction is completely defined by its one-particle density matrix (1PDM)[6], and thus 1PDMs and wavefunctions will be used interchangeably throughout. EDA schemes have also been defined for various post-HF wavefunction theories[7–12], but these will not be considered further here.

There are many EDA schemes but currently only a handful of distinct ways used to construct the initial supersystem wavefunction. The simplest choice is to adopt the Hartree product of monomer wavefunctions as the initial supersystem electronic wavefunction despite its lack of proper antisymmetry with respect to electron variables. This approach is employed by methods such as the polarization theory[8], Kitaura-Morokuma EDA (KM-EDA)[13–15], pair interaction energy decomposition analysis (PIEDA)[16,17], and configuration analysis for fragment interaction (CAFI)[18], which are older methods or are adapted from older methods. These approaches, except for the polarization theory, which is only valid for well-separated fragments, eventually account for antisymmetry in the supersystem wavefunction but not until after a classical polarization procedure has been performed.

A majority of EDAs employ the antisymmetric product of isolated monomer wavefunctions (i.e. "frozen" fragment orbitals), the Heitler-London wavefunction, as the initial supersystem wavefunction to define what is therefore often called the frozen energy. Such EDAs include symmetry adapted perturbation theory (SAPT)[8,19–22], Bickelhaupt-Baerends EDA (BB-

[a)] Electronic mail: prhorn@berkeley.edu
[b)] Electronic mail: mhg@cchem.berkeley.edu

EDA)[2,23,24], the natural orbitals for chemical valence method combined with the extended transition state method (NOCV-ETS)[25–28], generalized Kohn-Sham EDA (GKS-EDA)[29–31], the constrained space orbital variation method (CSOV)[32], the reduced variational space method (RVS)[15,33], the configuration interaction (CI)-singles based scheme of Reinhardt et al.[34], the method of De Silva and Korchowiec[35], the method of Mandado and Hermida-Ramón[36], block-localized wavefunction EDA (BLW-EDA)[3,37,38] (though not so obviously in later works[39]), and absolutely localized molecular orbital EDA (ALMO-EDA)[40–43]. Another method, natural EDA (NEDA)[1,44–47], also uses the antisymmetric product though not of the isolated monomer wavefunctions but rather of the natural bond orbital (NBO)-determined monomer Lewis-like determinants.

A refreshingly different definition for the initial supersystem wavefunction is used in the density-based EDA (DEDA) scheme of Wu et al.[48,49] The DEDA method uses constrained DFT to define the initial wavefunction as the lowest energy single Slater determinant that has a 3-space density equivalent to the sum of isolated fragment densities. The DEDA is the first EDA to add an energetic optimality condition to the construction of the initial supersystem wavefunction while still making a connection to the properties of isolated fragments. Constant density minimization can lower the DFT energy because it depends on the 1PDM through at least the kinetic energy, and the mapping between 1PDMs and densities is many-to-one by virtue of linear dependence in the products of basis functions used to construct the density matrix[50].

For the DEDA examples presented by Wu et al.[48,49], minimization with constant sum of fragments density yielded very significant energy lowering beyond the frozen orbital energy used in EDAs such as Bickelhaupt-Baerends EDA, BLW-EDA, and ALMO-EDA. For example, for the water dimer using B3LYP/aug-cc-pVQZ at R_e, the frozen orbital interaction energy is -7.6 kJ/mol, while the DEDA approach yields a frozen energy of -14.3 kJ/mol, relative to the total interaction energy of -19.0 kJ/mol. This means that the post-frozen contribution of polarization and charge transfer is reduced by more than a factor of two in DEDA versus the conventional EDA approaches, from 11.4 kJ/mol to 4.6 kJ/mol. Thus the choice of frozen energy has important consequences for the interpretative purposes of the EDA, and the DEDA casts possible doubt on the validity of the conventional EDAs.

Our goal is to understand the origin of the large energetic differences between the DEDA frozen energy and that obtained using the frozen orbitals. Is it primarily intra-fragment relaxation that relieves steric repulsions, without changing the density? Or is it instead dominated by inter-fragment relaxation, corresponding to CT at constant density? For EDA purposes, it is essential to distinguish these two cases, since CT is separated from the electrostatic, Pauli and dispersion interactions associated with the frozen energy. On the other hand, there are other applications of the frozen energy, such as parameterizing force field models[51] that lack explicit CT terms, where it may be desirable to include the constant density CT in the frozen energy to minimize the magnitude of the separate CT term. Thus the merit of a particular frozen energy definition must be assessed on the basis of the intended application.

To explore this issue, we shall consider four alternative frozen energies, summarized in Table I and outlined in detail in Sec. II below. The basic method, denoted as $P_{\rm frz}$, evaluates the energy associated with the frozen orbitals of the isolated fragments, without further optimization. This energy can be lowered variationally by performing a constrained self-consistent field (SCF) minimization at constant density, denoted as $\rho_{\rm frz}$-SCF if the density corresponding to $P_{\rm frz}$ is used, or as $\rho_{\rm sum}$-SCF if the sum of fragment densities is used. The latter is the DEDA frozen energy. In order to distinguish the relaxation due to constant density polarization from that due to constant density CT, we define the $\rho_{\rm frz}$-SCFMI frozen energy, which excludes CT effects from the constrained minimization using a recently developed variant of the SCF for molecular interactions (SCFMI)[52]. After validating our approach to approximately satisfying the constant density constraint, we then compare the results from these four models on the repulsive part of the neon dimer potential curve, the water dimer, ammonia borane, and ethane dissociation.

II. MODELS FOR THE INITIAL SUPERSYSTEM WAVEFUNCTION

General notation in this work is as follows: subspace indices: capital Roman $X, Y...$; AO basis indices: lower case Greek μ, $\nu...$; virtual MO indices: $a, b...$; occupied MO indices: $i, j...$; generic MO indices: $r, s.....$ This work considers nonorthogonal subspaces and thus makes use of tensors with both covariant (subscript) and contravariant (superscript) indices.[53] Further notation will be introduced as needed.

Method	Energy	P_{target}	Optimization
P_{frz}	$E^{\text{frz}}_{\text{initial}}$	P_{frz}	none
ρ_{sum}-SCF	$E^{(\text{sum,SCF})}_{\text{initial}}$	$\sum_A P_A$	SCF (intra+inter)
ρ_{frz}-SCF	$E^{(\text{frz,SCF})}_{\text{initial}}$	P_{frz}	SCF (intra+inter)
ρ_{frz}-SCFMI	$E^{(\text{frz,SCFMI})}_{\text{initial}}$	P_{frz}	SCFMI (intra)

TABLE I: Four methods to compute the frozen energy. P_{target} is the density matrix which defines the 3-space density constraint, and optimization indicates which orbital degrees of freedom are varied during constant density minimization. The energy is that of the initial supersystem wavefunction, which, together with the common isolated monomer energies, determines the frozen energy. The frozen energy method labeled P_{frz} is used in the ALMO-EDA and most others and involves no energy optimization. The frozen energy method labeled ρ_{sum}-SCF is used in Wu's DEDA[48,49].

A. The Frozen Orbital Model (P_{frz})

To guarantee a valid single Slater determinant wavefunction from which a valid energy can be evaluated, the most basic model simply uses the frozen orbitals of each fragment. They are non-orthogonal from one fragment to the next, and therefore a valid one-particle density matrix must include the appropriate metric:

$$\mathbf{P}_{\text{frz}} = \mathbf{C}^{\text{occ}}_{\text{frz}} \sigma^{-1} (\mathbf{C}^{\text{occ}}_{\text{frz}})^{\dagger} \tag{II.1}$$

$$\sigma = (\mathbf{C}^{\text{occ}}_{\text{frz}})^{\dagger} \mathbf{S} \mathbf{C}^{\text{occ}}_{\text{frz}} \tag{II.2}$$

The occupied MO coefficient matrices of the isolated fragments, $\{\mathbf{C}^{\text{occ}}_A\}$, comprise the diagonal blocks of $\mathbf{C}^{\text{occ}}_{\text{frz}}$, while off-diagonal blocks are zero:

$$\mathbf{C}^{\text{occ}}_{\text{frz}} = \begin{bmatrix} \mathbf{C}^{\text{occ}}_A & \mathbf{0} & \cdots \\ \mathbf{0} & \mathbf{C}^{\text{occ}}_B & \\ \vdots & & \ddots \end{bmatrix} \tag{II.3}$$

The frozen orbital density matrix, Eq. II.1, is equivalent to the density matrix for the single determinant Heitler-London wavefunction built as the antisymmetric product of subsystem Slater determinants. The frozen orbital density matrix in turn yields a frozen density as $\rho_{\text{frz}}(\mathbf{r}) = P_{\text{frz}}(\mathbf{r}, \mathbf{r})$, as well as the energy corresponding to the frozen orbital initial supersystem wavefunction: $E^{\text{frz}}_{\text{initial}} = E(\mathbf{P}_{\text{frz}})$. The frozen energy is obtained (for all models) by subtracting the sum of isolated monomer energies from that of the initial supersystem wavefunction.

$$E^{\text{frz}}_{\text{FRZ}} = E^{\text{frz}}_{\text{initial}} - \sum_A E_A \tag{II.4}$$

An equivalent derivation of the projector corresponding to Eq. II.1 begins with the formation of the sum of the occupied subspace projectors for the isolated subsystems, $\mathbf{P}_{\text{sum}}$. $\mathbf{P}_{\text{sum}}$ is not generally a valid projector, as the sum of non-orthogonal projectors is not a projector (i.e. its eigenvalues deviate from 0 and 1). The idempotent projector that is closest to this simple sum may be found by successive applications of the well-known McWeeny purification[54] beginning with $\mathbf{P}^{(0)} = \mathbf{P}_{\text{sum}}$:

$$\mathbf{P}^{(i+1)} = \mathbf{3P}^{(i)}\mathbf{SP}^{(i)} - \mathbf{2P}^{(i)}\mathbf{SP}^{(i)}\mathbf{SP}^{(i)} \tag{II.5}$$

It has been proven that the final result of that sequence, $\mathbf{P}^{(\infty)}$, is geometrically optimal, in the sense of being the closest valid projector to $\mathbf{P}_{\text{sum}}$ in the space of matrices[55]. It is moreover straightforward to prove that under mild conditions $\mathbf{P}_{\text{frz}} = \mathbf{P}^{(\infty)}$.

The frozen orbital density matrix thus defines a geometrically optimal initial supersystem wavefunction, and its corresponding $\rho(\mathbf{r})$ will be in non-trivial cases different from the sum of subsystem densities. The distortion of this density relative to the simple sum is a consequence of the requirement for an antisymmetric electronic wavefunction, and its qualitative features been discussed in detail by other authors[23]. Briefly, the distortions include a depletion of electron density in the overlapping region and an increase in electron density near nuclei, resulting in higher electron kinetic energy and lower electron-nuclear potential energy.

B. Energy minimization with the sum of fragment densities constraint (ρ_{sum}-SCF)

This approach is the basis of Wu's Density-based Energy Decomposition Analysis (DEDA)[48,49]. Imagine translating the electron densities of the subsystems along with their respective nuclei from infinitely far away to the supersystem geometry, resulting in a supersystem 3-space electron density, $\rho_{\text{sum}}(\mathbf{r})$, that is the sum of subsystem densities:

$$\rho_{\text{sum}}(\mathbf{r}) = \sum_A \rho_A(\mathbf{r}) \tag{II.6}$$

The correct number of electrons is obtained. This method appears classical because it discounts elec-

tronic wavefunction antisymmetry, and it is the classical electrostatic interaction between these translated nuclei and electron densities that is used to define the permanent electrostatic interaction energy component in some EDAs.

Is there, by extension, a valid supersystem occupied subspace projector that is a sum of subsystem occupied subspace projectors? The sum of projectors is only a projector if the respective vectors defining the spans are orthogonal from one span to the next or equivalently if the metric for the collection of these vectors is subspace-block-diagonal. This is trivially true for non-overlapping (i.e. very weakly interacting) fragments and *can* also be true in the strongly interacting case. For example one could re-partition $\rho_{\text{sum}}(\mathbf{r})$ into *non-overlapping* spatial domains corresponding to each fragment, with each having its original number of electrons, as illustrated schematically for a symmetric helium-dimer-like system in Figure 1. This will enable subsystem projectors to be strongly orthogonal, and it is a feasible point on the idempotent surface, at least in a complete basis set. By contrast, in a minimal basis for two overlapping He atoms, such a feasible point does not exist. We believe the question of whether or not feasible points strictly exist in larger finite basis sets is open.

Wu employs constrained DFT to compute the lowest energy single Slater determinant for the supersystem with the constraint that its corresponding $\rho(r)$ equals the sum of isolated fragment densities:

$$E_{\text{initial}}^{(\text{sum,SCF})} = \underset{\rho_{\text{sum}} \leftarrow \mathbf{P}}{\text{minimize}}\, E\left[\mathbf{P}\right] \qquad \text{(II.7)}$$

There are two interesting issues with this approach. The first, already discussed above, is that if a feasible solution does not exist, then the constrained DFT algorithm does not impose a constraint, but instead adds an energetic penalty that enforces similarity between the actual 3-space density of the wavefunction and $\rho_{\text{sum}}(\mathbf{r})$. The second interesting issue, already discussed in the Introduction, is the question of the interpretation of the energy lowering associated with a wavefunction optimized in such a way. The next two definitions will help to address this latter issue.

C. Energy minimization with the frozen orbital density constraint (ρ_{frz}-SCF)

The issue of existence or non-existence of valid projectors yielding ρ_{sum} in Wu's density matching constraint can be circumvented by instead requiring

FIG. 1: Sum of densities, ρ_{sum}, for a helium dimer system, showing a sharp division into two fragment quantities in the overlapping regime. This sharp division is a feasible point, in the sense that it can be represented by two localized orthogonal orbitals, in a complete basis set. It is not a feasible point in a finite basis set, such as a minimal basis, composed of smooth functions.

the density to match the frozen orbital density, ρ_{frz}, in a constrained minimization of the frozen energy:

$$E_{\text{initial}}^{(\text{frz,SCF})} = \underset{\rho_{\text{frz}} \leftarrow \mathbf{P}}{\text{minimize}}\, E\left[\mathbf{P}\right] \qquad \text{(II.8)}$$

The result of this minimization is necessarily an energy lowering relative to the frozen orbital energy, and various numerical tests of this energy difference will be presented later. Relative to energy minimization constrained to ρ_{sum}, the optimized energy, $E_{\text{initial}}^{(\text{frz,SCF})}$, could be either higher or lower, a fact that will be confirmed with numerical examples. In both cases, the constant density relaxation must be viewed as including both intra-fragment and inter-fragment contributions.

D. Energy minimization with constrained density and without charge transfer (ρ_{frz}-SCFMI)

The main issue with constant density minimization of the frozen energy is the origin of the energy lowering in the context of other EDA terms. We wish

to distinguish contributions due to intra-fragment relaxation from those due to inter-fragment relaxation, because the latter is CT in character. Constant density minimization requires an additional constraint to prohibit CT between fragments. The SCFMI constraint of a fragment-blocked AO to MO coefficient matrix[40,56–60] has often been used to describe polarization and exclude CT[3,37,38,41–43]. Fragment-blocking retains the form of the MO coefficients, (II.3), associated with the frozen-orbital density matrix, (II.1), which is thus the natural initial guess. Use of ρ_{frz} for the density constraint is also natural, since we are guaranteed the initial feasible point, $\mathbf{P}_{\text{frz}}$.

However, SCFMI in the AO basis does not converge to a useful complete basis set (CBS) limit for polarization. SCFMI captures more and more of the CT contribution as the AO basis set size increases[52,61]. To address this problem, as well as to generalize the SCFMI method to representations (such as plane waves) where the underlying basis is not fragment-blocked, we recently developed a polarization basis composed of fragment electric-field response functions (FERFs)[52]. The FERFs that exactly describe the fragment linear response to a uniform electric field comprise 3 dipolar (D) functions per occupied fragment orbital. Similarly, 5 additional quadrupolar (Q) FERFs describe the fragment linear response to an electric field gradient. Numerical tests showed that the non-orthogonal D+Q polarization model (nDQ) satisfactorily reproduced exact results for polarization in the non-overlapping limit, while also maintaining a non-trivial basis set limit in the overlapping regime.

Constant density minimization without CT can thus be accomplished via density constrained minimization within the SCFMI/nDQ model[52]:

$$E_{\text{initial}}^{(\text{frz,SCFMI})} = \underset{\rho_{\text{frz}} \leftarrow \mathbf{P};\ \text{SCFMI/nDQ}}{\text{minimize}} E\left[\mathbf{P}\right] \quad \text{(II.9)}$$

The 3-space density constraint employed is for the total spinless density. It is the simplest option and allows the method to be defined for all single Slater determinant methods. By virtue of the SCFMI constraint, (II.9) satisfies:

$$E_{\text{initial}}^{\text{frz}} \geq E_{\text{initial}}^{(\text{frz,SCFMI})} \geq E_{\text{initial}}^{(\text{frz,SCF})} \quad \text{(II.10)}$$

Wu *et al*'s results[48,49] suggest that the difference $E_{\text{initial}}^{\text{frz}} - E_{\text{initial}}^{(\text{frz,SCF})}$ is significant (technically they evaluated $E_{\text{initial}}^{\text{frz}} - E_{\text{initial}}^{(\text{sum,SCF})}$ instead). $E_{\text{initial}}^{(\text{frz,SCFMI})}$ *partitions this difference into intrafragment and interfragment contributions.*

By virtue of the constant density constraint, (II.9) also satisfies:

$$E_{\text{initial}}^{\text{frz}} \geq E_{\text{initial}}^{(\text{frz,SCFMI})} \geq E_{\text{SCFMI}} \quad \text{(II.11)}$$

The fact that $E_{\text{initial}}^{(\text{frz,SCFMI})} \geq E_{\text{SCFMI}}$ ensures a negative semi-definite value for the polarization energy ($E_{\text{POL}} = E_{\text{SCFMI}} - E_{\text{initial}}$) when using the ρ_{frz}-SCFMI model for the frozen energy. (II.9) differs from the usual initial supersystem energy, $E_{\text{initial}}^{\text{frz}}$, typically used in EDAs, because it prevents constant density intrafragment relaxation from later being counted toward the polarization term. Polarization that does not change the density is by definition not polarization at all. Instead it is an indicator of an energetic inadequacy in the initial supersystem wavefunction. $E_{\text{initial}}^{(\text{frz,SCFMI})} - E_{\text{initial}}^{\text{frz}}$ *measures this inadequacy.*

III. IMPLEMENTATION

A. Methodology for Computing the Initial Supersystem Wavefunction

The nonlinear problem defined by (II.9) is a minimization of the single determinant electronic energy of a system with both SCFMI and constant density constraints. Methods for SCFMI optimization are well known[40,52,56,59,62,63]. However, the proper parameters for optimization on the surface of constant $\rho(\mathbf{r})$ let alone those for the surface defined by the intersection of the SCFMI constraint and constant $\rho(\mathbf{r})$ are not known.

We therefore resort to the use of Lagrange multipliers and define the following penalty function:

$$E_{\text{penalty}}\left[\delta\mathbf{P}\right] = \frac{1}{2}\delta P^{\mu\nu}\left(\mu\nu|\lambda\sigma\right)\delta P^{\lambda\sigma} \quad \text{(III.1)}$$

$$\left(\mu\nu|\lambda\sigma\right) = \iint \omega_\mu(1)\omega_\nu(1)r_{12}^{-1}\omega_\lambda(2)\omega_\sigma(2)d\mathbf{r}_1 d\mathbf{r}_2 \quad \text{(III.2)}$$

The deviation in the density matrix, $\mathbf{P}$, is defined as $\delta\mathbf{P} = \mathbf{P} - \mathbf{P}_{\text{target}}$, where $\mathbf{P}_{\text{target}}$ produces the target density, $\rho_{\text{target}}\left(\mathbf{r}\right) = P_{\text{target}}\left(\mathbf{r},\mathbf{r}\right)$. The energy penalty is the coulomb interaction of the density error, $\delta\rho(\mathbf{r})$, with itself, and it will be zero when the densities are identical.

We can write a Lagrangian for this constrained optimization problem with a single Lagrange multiplier, λ, as:

$$\mathcal{L}\left[\mathbf{P},\lambda\right] = E\left[\mathbf{P}\right] + \lambda E_{\text{penalty}}\left[\delta\mathbf{P}\right] \quad \text{(III.3)}$$

where E is the usual electronic energy as defined by Hartree-Fock or some Kohn-Sham density functional with at most 1PDM dependence. Stationarity with respect to λ requires that (III.1) be zero. We can solve this optimization problem using an outer loop that monotonically increases λ, which is ideally infinite but is in practice chosen to be sufficiently large such that the penalty function (III.1) is zero to within tolerance. An inner loop solves for the optimal $\mathbf{P}$ by (III.3) at fixed λ and of course fixed $\mathbf{P}_{\text{target}}$.

The relevant partial derivatives for the optimization at fixed λ are:

$$(F_\lambda)_{\mu\nu} \equiv \frac{\partial \mathcal{L}}{\partial P^{\mu\nu}} = F_{\mu\nu} + \lambda (F_{\text{penalty}})_{\mu\nu} \qquad \text{(III.4)}$$

$$(F_{\text{penalty}})_{\mu\nu} = (\mu\nu|\lambda\sigma)\, \delta P^{\lambda\sigma} \qquad \text{(III.5)}$$

The above expression for $\mathbf{F}_\lambda$, (III.4), can be used in place of the normal density derivative of the electronic energy, $\mathbf{F}$, in standard gradient- or eigenvalue-based nonlinear solvers to obtain the optimal $\mathbf{P}$ at fixed λ where $\mathbf{P}$ has either full SCF[64,65] or SCFMI[52,56,59] degrees of freedom.

Because of the difficulty in converging the constant λ problem for λ large, the protocol employed in this work consists of a combination of two algorithms. The first is preconditioned limited-memory Broyden-Fletcher-Goldfarb-Shanno (L-BFGS)[66] using orbital rotation parameters[52,64,67] and employing a robust line search[68]. The preconditioner used for both surfaces considered is all of $\mathbf{F}_\lambda \cdot \mathbf{P}^{\Delta\Delta}$, which in the case of SCF can be written in terms of $\mathbf{F}_\lambda$ occupied-virtual eigenvalue differences after pseudocanonical transformation and in the case of SCFMI involves a series of nested preconditioned linear equations that have been described previously[52]. The second algorithm, used ideally for only a single step after the first algorithm has converged to a modest tolerance, is Newton-Raphson. The linear equation for the solution of the Newton step by conjugate gradient is generally poorly conditioned, but it can be adequately solved if λ is not too large.

The Hessian-vector-product needed in the conjugate gradient iterations for the solution of the Newton step (as well as for the determination of the FERF subspaces[52]) can either be computed analytically or by finite difference[69] (with an orbital displacement of order 1.0×10^{-4}) when second functional derivatives are not available. In the former case, the second density derivative of the Lagrangian (III.3) with respect to the density matrix is needed.

$$\frac{\partial^2 \mathcal{L}}{\partial P_\alpha^{\mu\nu} \partial P_\beta^{\pi\sigma}} = (\Pi_{\alpha\beta})_{\mu\nu\pi\sigma} + \lambda\, (\mu\nu|\pi\sigma) \qquad \text{(III.6)}$$

$$(\Pi_{\alpha\beta})_{\mu\nu\lambda\sigma} \equiv \frac{\partial^2 E}{\partial P_\alpha^{\mu\nu} \partial P_\beta^{\lambda\sigma}} \qquad \text{(III.7)}$$

The tensor $\mathbf{\Pi}$ involves the two electron integrals and second functional derivatives of the exchange correlation energy in the case of DFT. In practice, the Lagrangian first (III.4) and second (III.6) density derivatives are simply used in place of $\mathbf{F}$ and $\mathbf{\Pi}$ respectively in the usual expressions for the Hessian with respect to electronic degrees of freedom.[52,70]

We use this method based on the coulomb interaction of the density error with itself instead of the constrained DFT approach[48] to the constant $\rho(r)$ constraint for two reasons. It is straightforward to implement, and it has a single parameter, λ, which can be used to increase the fidelity of the 3-space density matching as opposed to the many parameters present in the additional basis expansion of the constraint potential that are necessary in DEDA. In principle either approach can exactly enforce the constraint, but in practice, due to computational limitations, neither will, and so some validation will be necessary.

There are several measures of the deviation of the optimized density from the constant $\rho(\mathbf{r})$ surface. One possibility is the penalty function itself (III.1) though this has little physical relevance. Another with the meaning of displaced electrons[49] is the integral of the absolute value of the deviation in the density:

$$\epsilon_\rho = \int_{\mathbf{r}} |\rho(\mathbf{r}) - \rho_{\text{target}}(\mathbf{r})| \qquad \text{(III.8)}$$

However, what is perhaps most meaningful in assessing constant $\rho(\mathbf{r})$ relaxation is a measure with units of energy. Both the electron-nuclear attraction and electron-electron repulsion (coulomb) energies should remain constant during constant $\rho(\mathbf{r})$ density relaxation. Thus, the changes in these contributions give an estimate of the portion of the energy change upon relaxation that is illegitimate, deriving from (small) changes in $\rho(\mathbf{r})$ that violate the constant density constraint due to finite λ etc.

B. Computational Details

Calculations in this work were performed with a development version of QChem[71,72]. The SCFMI

subspaces used to compute the $\rho_{\rm frz}$-SCFMI model are non-orthogonal FERF DQ subspaces, which have been described previously[52]. The FERF models do not have the weakness of a trivial basis set limit that simple fragment-AO-blocked SCFMI schemes possess. The aug-cc-pVQZ basis of Dunning[73,74] is used for all single point calculations both because it allows direct comparison with previously reported results of Wu in some cases and because this basis has been shown to be adequate for the construction of FERF DQ subspaces[52]. All single point calculations employ the B3LYP[75–77] functional likewise for direct comparison but also because it is in common use with deficiencies mainly in its description of dispersive intermolecular interactions, which are not of primary interest in this work. No corrections for basis set superposition error were performed because aug-cc-pVQZ is sufficiently large that BSSE effects are negligible. If a much smaller basis set were used, constant density relaxation would be diminished due to the decreased number of linearly dependent basis function products, and it would also become more difficult to find a density matrix that collapses to $\rho_{\rm sum}$. Using FERFs (rather than AOs) to define the SCFMI subspaces would also become less necessary. For calculations involving constant density constraints, the energy values reported are for λ = 2000 a.u. unless otherwise indicated.

IV. VALIDATION OF CONSTANT DENSITY CONSTRAINT ALGORITHM

The purpose of this section is to validate our method of optimizing single Slater determinant wavefunctions with approximate enforcement of the constraint of a fixed $\rho(\mathbf{r})$. We aim to establish the size of the errors due to inexact constraint satisfaction so that we can later be sure that such errors are smaller than the differences between the four different initial supersystem wavefunction definitions compared in Section V.

We begin with the neon dimer because DEDA results are available[49] using both a large (aug-cc-pVQZ) potential basis set (PBS) as well as a complete (potential) basis set (CBS) limit extrapolation procedure. The difference between Wu's aug-cc-pVQZ PBS result for the frozen energy (273.76 kJ/mol) and that obtained using the finite Lagrange multiplier coulomb penalty method with identical constraints, $\rho_{\rm sum}$-SCF, for λ=2000 is 0.53 kJ/mol at $R = 1.59$Å (3.0 Bohr) with our computed frozen energy slightly higher. This suggests that we have done a slightly better job of enforcing the constant density constraint in this case. The difference between the results of the two algorithms at 2.12 Å (4.0 Bohr) separation is reduced to 0.13 kJ/mol with constrained DFT producing the higher energy. Because the difference between the algorithms and the magnitude of $E_{\rm FRZ}^{\rm (frz,SCF)}$ are both considerably smaller at this larger separation, further analysis for the neon dimer will focus on the internuclear separation of 1.59 Å.

The Lagrange multiplier of λ=2000 is used throughout this work (with a few noted exceptions) as it is a fairly large value for which the optimization problem at fixed λ could be reliably converged for all methods for most of the systems investigated . We now consider convergence of the $\rho_{\rm sum}$-SCF frozen energy with respect to λ at a single point (R_{Ne-Ne} = 1.59 Å= 3.0 Bohr) on the neon dimer potential energy surface to place this computational limitation into perspective. Figure 2 shows both integrated absolute density errors, ϵ_ρ, (Figure 2a) and relative frozen energies (Figure 2b) for a range of λ values between 500 and 3000.

Figure 2a shows slow convergence of the integrated density error with respect to λ, with a polynomial decay of roughly $\lambda^{-0.5}$. However, the ϵ_ρ error measure that we compute for our finite λ=2000 calculation of the $\rho_{\rm sum}$-SCF model is more than five times smaller than the same value reported by Wu[49] based on his constrained DFT method with an aug-cc-pVQZ PBS. Based on these results and the energies discussed above, we conclude that our methodology for performing constrained optimizations with fixed $\rho(\mathbf{r})$ is capable of at least the same accuracy as Wu's scheme with the largest potential basis set that he has employed.

Figure 2b shows the $\rho_{\rm sum}$-SCF frozen energy as computed using the coulomb penalty algorithm for $\lambda \geq 500$ relative to the λ=500 value. This figure shows that, like ϵ_ρ, the initial wavefunction energy also converges quite slowly with respect to λ. Included as well are the finite and complete potential basis set results from Wu[49] using constrained DFT. Our $\rho_{\rm sum}$-SCF value with λ=3000 has already passed Wu's CBS extrapolated value for the same model, and we can be sure that the energy will rise further still for larger values of λ.

Next, we consider an extrapolation of the $\rho_{\rm sum}$-SCF frozen energy to the ϵ_ρ=0 limit for the purpose of assessing errors in our finite λ=2000 calculations. The result of applying linear regression to the relative $E_{\rm FRZ}$ vs ϵ_ρ curve based on the data presented in Figures 2a and 2b is displayed in Figure 2c. The corresponding ϵ_ρ=0 extrapolated value relative to the

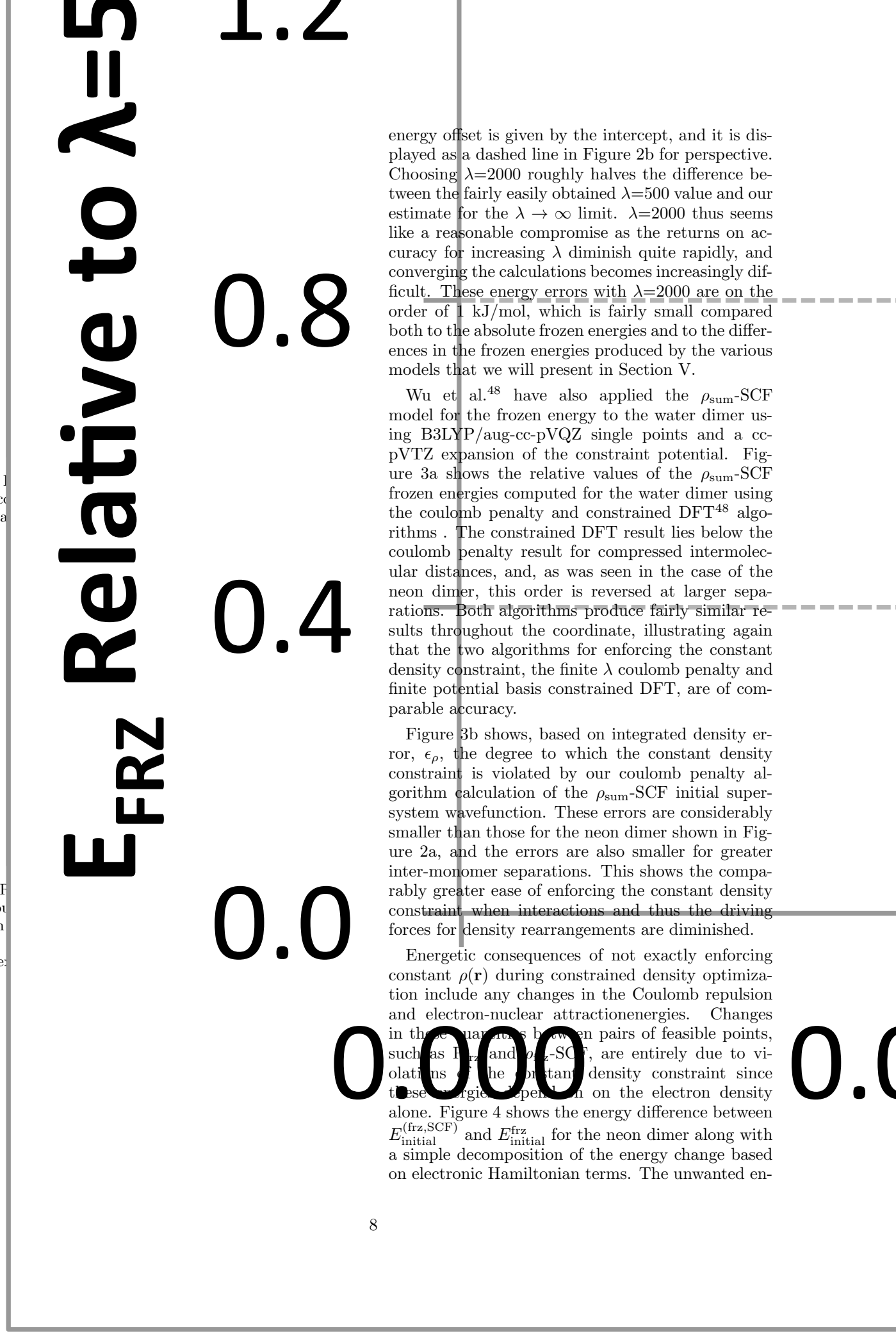

energy offset is given by the intercept, and it is displayed as a dashed line in Figure 2b for perspective. Choosing λ=2000 roughly halves the difference between the fairly easily obtained λ=500 value and our estimate for the $\lambda \to \infty$ limit. λ=2000 thus seems like a reasonable compromise as the returns on accuracy for increasing λ diminish quite rapidly, and converging the calculations becomes increasingly difficult. These energy errors with λ=2000 are on the order of 1 kJ/mol, which is fairly small compared both to the absolute frozen energies and to the differences in the frozen energies produced by the various models that we will present in Section V.

Wu et al.[48] have also applied the ρ_{sum}-SCF model for the frozen energy to the water dimer using B3LYP/aug-cc-pVQZ single points and a cc-pVTZ expansion of the constraint potential. Figure 3a shows the relative values of the ρ_{sum}-SCF frozen energies computed for the water dimer using the coulomb penalty and constrained DFT[48] algorithms . The constrained DFT result lies below the coulomb penalty result for compressed intermolecular distances, and, as was seen in the case of the neon dimer, this order is reversed at larger separations. Both algorithms produce fairly similar results throughout the coordinate, illustrating again that the two algorithms for enforcing the constant density constraint, the finite λ coulomb penalty and finite potential basis constrained DFT, are of comparable accuracy.

Figure 3b shows, based on integrated density error, ϵ_ρ, the degree to which the constant density constraint is violated by our coulomb penalty algorithm calculation of the ρ_{sum}-SCF initial supersystem wavefunction. These errors are considerably smaller than those for the neon dimer shown in Figure 2a, and the errors are also smaller for greater inter-monomer separations. This shows the comparably greater ease of enforcing the constant density constraint when interactions and thus the driving forces for density rearrangements are diminished.

Energetic consequences of not exactly enforcing constant $\rho(\mathbf{r})$ during constrained density optimization include any changes in the Coulomb repulsion and electron-nuclear attractionenergies. Changes in these quantities between pairs of feasible points, such as E_{frz} and ρ_{frz}-SCF, are entirely due to violations of the constant density constraint since these energies depend on the electron density alone. Figure 4 shows the energy difference between $E^{(\text{frz,SCF})}_{\text{initial}}$ and $E^{\text{frz}}_{\text{initial}}$ for the neon dimer along with a simple decomposition of the energy change based on electronic Hamiltonian terms. The unwanted en-

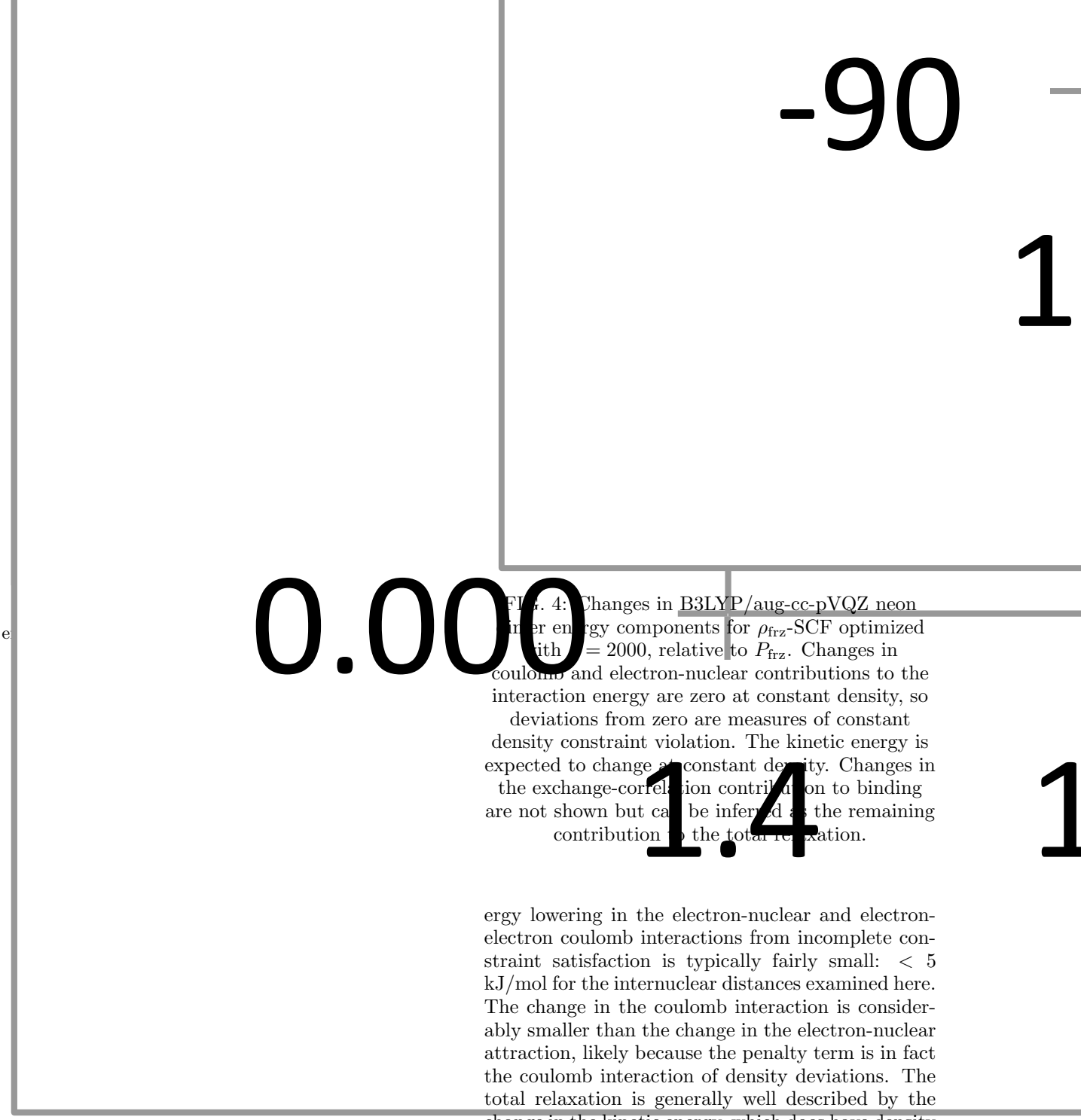

(b) Density error, ϵ_ρ, for the B3LYP/aug-cc-pVQZ ρ_{sum}-SCF initial supersystem wavefunction computed using the J penalty algorithm as a function of the H-bond coordinate.

FIG. 3: Assessment of the B3LYP/aug-cc-pVQZ ρ_{sum}-SCF frozen energy computed by the λ=2000 coulomb penalty algorithm (J penalty) and previously reported cc-pVTZ potential basis set constrained DFT results from Wu et al.[48] (Wu TZ). The system is the MP2/aug-cc-pVQZ optimized and rigidly displaced water dimer at various H-bond (R_{O-H}) distances.

FIG. 4: Changes in B3LYP/aug-cc-pVQZ neon dimer energy components for ρ_{frz}-SCF optimized with $\lambda = 2000$, relative to P_{frz}. Changes in coulomb and electron-nuclear contributions to the interaction energy are zero at constant density, so deviations from zero are measures of constant density constraint violation. The kinetic energy is expected to change at constant density. Changes in the exchange-correlation contribution to binding are not shown but can be inferred as the remaining contribution to the total relaxation.

ergy lowering in the electron-nuclear and electron-electron coulomb interactions from incomplete constraint satisfaction is typically fairly small: < 5 kJ/mol for the internuclear distances examined here. The change in the coulomb interaction is considerably smaller than the change in the electron-nuclear attraction, likely because the penalty term is in fact the coulomb interaction of density deviations. The total relaxation is generally well described by the change in the kinetic energy, which does have density matrix dependence. The remaining relaxation not displayed here is relatively small and corresponds to changes in the exchange-correlation energy.

In conclusion, the accuracy of our coulomb-based method for constant $\rho(\mathbf{r})$ energy minimization is at least comparable to that of Wu's constrained-DFT-based method. Inexact constraint satisfaction during constant density energy minimization lowers the frozen energy by on the order of 1 kJ/mol for Ne_2. Figures similar to Figure 4 appear in the SI for different systems, and they indicate that this single digit

kJ/mol error is typical in the strongly overlapping regime.

V. RESULTS

In what follows, the numerical values given for all frozen energy models employing constant density constraints, ρ_{sum}-SCF, ρ_{frz}-SCF, and ρ_{frz}-SCFMI, were computed using the coulomb penalty algorithm with λ=2000 as validated above. We will see that differences in the frozen energy computed by the four different definitions (Table I) are often considerably larger than the energetic errors due to inexact constraint satisfaction (which we have shown to be on the order of 1 kJ/mol). Thus, we will be able to draw meaningful conclusions from our numerical results about the qualitative differences between the various definitions (or the lack thereof). The Supplemental Material[78] contains data (Figures S1-S4) for each of the following examples, confirming this assertion.

A. Neon Dimer

We begin by examining the compressed neon dimer to compare the four different frozen energy models summarized in Table I. Figure 5 shows the B3LYP/aug-cc-pVQZ frozen energies computed for the neon dimer at repulsive inter-atomic distances, both in absolute terms (Figure 5a) and relative to the basic frozen orbital model, P_{frz}, for clearer illustration of differences (Figure 5b).

The total interaction energy for the neon dimer is also included in Figure 5 to highlight the considerable range in the computed non-frozen contributions to the interaction energy. At the most compressed geometry considered, the non-frozen contribution, the difference between the total interaction energy and the frozen energy component as determined by a given method, varies by more than a factor of five depending on which constraints are chosen for the initial wavefunction optimization!

The main conclusion that can be drawn from Figure 5b is that the restriction of the density matrix to the SCFMI surface even with a constant density constraint already in place is significant. Comparing the ρ_{frz}-SCF and ρ_{frz}-SCFMI curves shows that the inclusion of interfragment degrees of freedom in the density matrix optimization at constant $\rho = \rho_{\text{frz}}$ results in more than four times the energy lowering relative to the energy of P_{frz}, which has the same

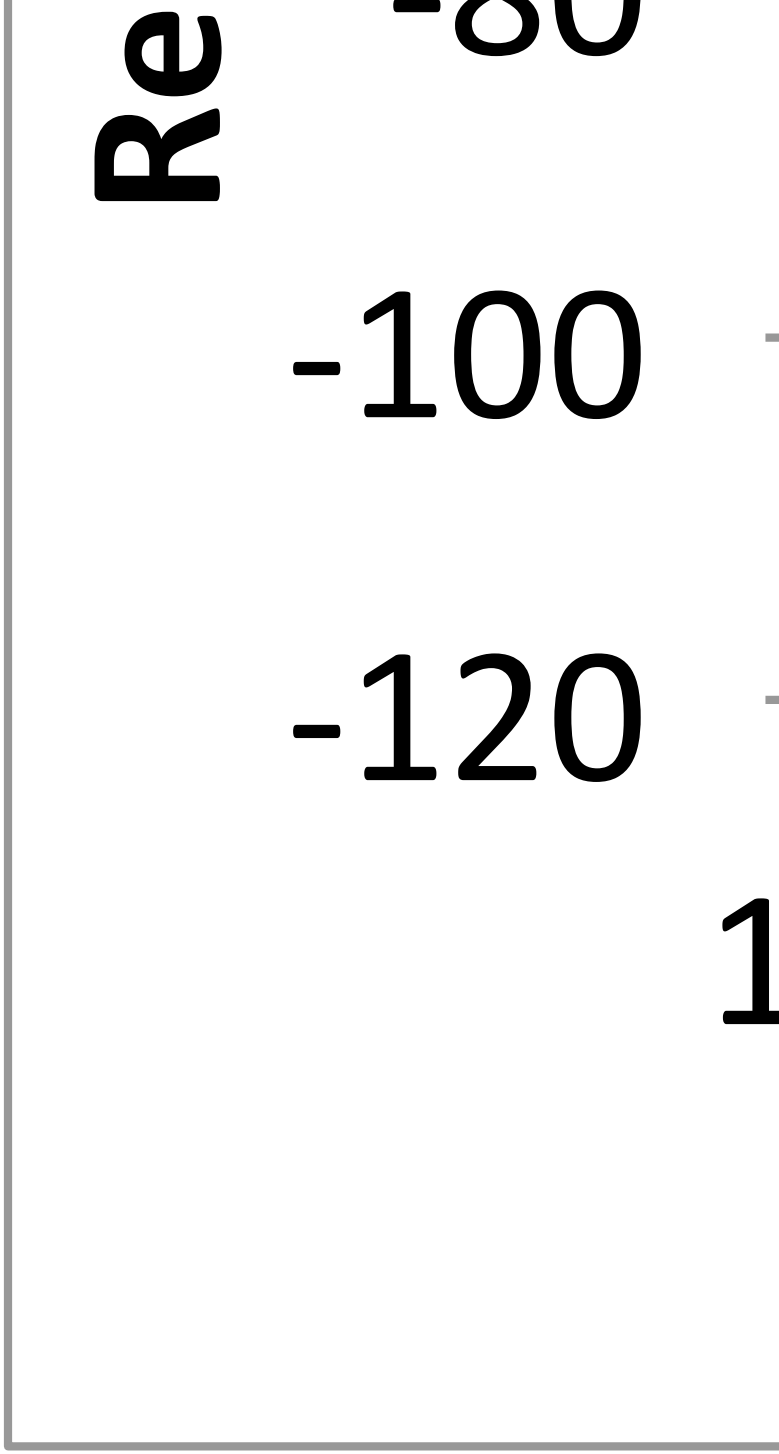

(b) Frozen energy deviations from the unoptimized P_{frz} value for several methods. ρ_{frz}-SCF and ρ_{frz}-SCFMI both correspond to relaxed wavefunctions relative to P_{frz}.

FIG. 5: Comparison of frozen energy models for B3LYP/aug-cc-pVQZ neon dimer at compressed internuclear distances ($R_e \sim 3.1$Å)

ρ_{frz}. Thus 80% of the energy lowering in ρ_{frz}-SCF can be identified as constant density charge transfer (CT) which dominates the much smaller energy lowering due to intrafragment relaxation.

From Figure 5b one can also see that despite the energetic optimality criterion present in the ρ_{sum}-SCF method, the corresponding energy is still considerably higher than that of the unoptimized frozen orbital density matrix, $\mathrm{P_{frz}}$, for the most repulsive coordinate values considered. ρ_{sum}-SCF does not have a meaningful unrelaxed analog and thus can be either higher or lower than $\mathrm{P_{frz}}$ in the overlapping regime. Indeed, the energetic ordering of the $\mathrm{P_{frz}}$ and ρ_{sum}-SCF methods is reversed at greater separations where the difference between the computed frozen energies drops below 0.5 kJ/mol.

B. Water Dimer

The water dimer is a fairly weakly interacting system for the displacements considered. Since charge transfer is known to contribute to the hydrogen bond[79–81], it is very interesting to see the extent to which constant density CT can help to lower the frozen energy during initial wavefunction optimization. Figure 6 shows results for the 4 frozen energy models (Figure 6a) as well as results offset relative to that of $\mathrm{P_{frz}}$ (Figure 6b). In this case, there is relatively little difference between the ρ_{sum}-SCF and ρ_{frz}-SCF results, suggesting that the target densities are roughly the same.

There is a clear distinction between the ρ_{frz}-SCF and ρ_{frz}-SCFMI schemes, indicating that the choice of orbital degrees of freedom is crucial. The ρ_{frz}-SCFMI scheme permits almost no relaxation relative to $\mathrm{P_{frz}}$, but the relaxation when all SCF orbital degrees of freedom are included is substantial on the scale of the interaction energy, approximately halving the non-frozen contribution to the interaction out to a separation of 2.6 Å. For example, at $\mathrm{R_{O-H}}$ = 2.0 Å, constant density interfragment relaxation decreases the non-frozen contribution from 11.16 to 5.76 kJ/mol.

The water dimer example demonstrates the importance of the SCFMI constraint during initial wavefunction optimization as it eliminates the substantial energy lowering associated with electron delocalization that is allowed in the ρ_{frz}-SCF and ρ_{sum}-SCF methods and thus the DEDA scheme. This contribution is properly part of CT in an EDA. This example also illustrates that for weakly interacting systems near or beyond the equilibrium separation, the energy lowering from constant density polariza-

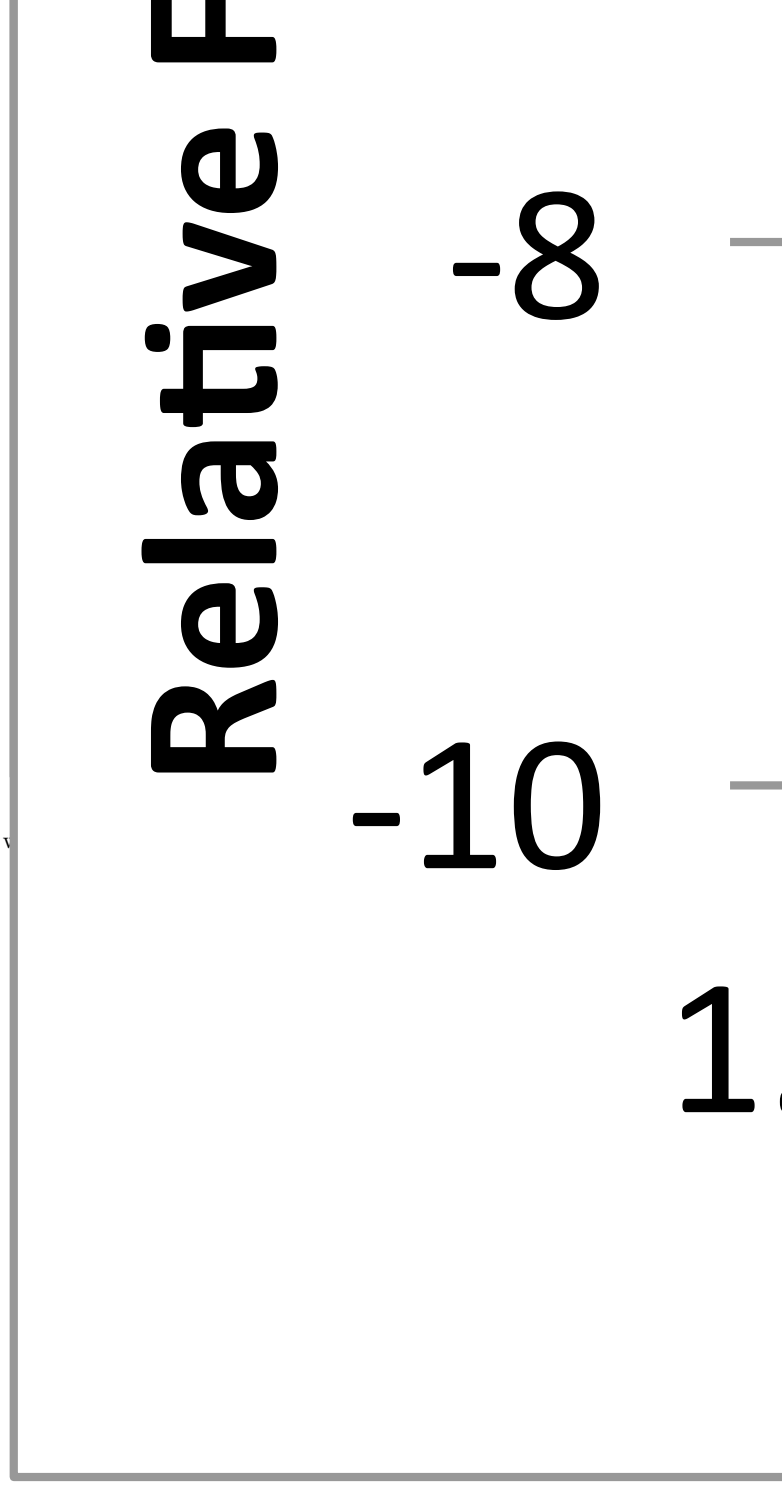

(b) Frozen energy component deviations from that of the frozen orbital density matrix for several methods.

FIG. 6: Comparison of the B3LYP/aug-cc-pVQZ frozen energies for the MP2/aug-cc-pVQZ optimized and rigidly displaced water dimer at various hydrogen bond ($\mathrm{R_{O-H}}$) distances.

tion, the difference between the frozen energy as computed by the P_{frz} and ρ_{frz}-SCFMI schemes, is negligible. It thus seems unnecessary to perform the ρ_{frz}-SCFMI initial wavefunction optimization to remove constant density polarization in the case of the water dimer.

C. Ammonia Borane Complex

The ammonia borane complex is included to assess whether systems more strongly interacting than the water dimer can display significant constant density relaxation even with the SCFMI orbital rotation constraint in place. The ammonia borane structures considered were obtained by a B3LYP/aug-cc-pVTZ relaxed scan of the R_{N-B} coordinate (equilibrium $R_{N-B} = 1.66$ Å at this level of theory).

Figure 7 shows absolute (Figure 7a) and relative (Figure 7b) frozen energies as computed by the various initial wavefunction methods. The relaxation relative to the energy of the frozen orbitals, P_{frz}, is considerably larger for the methods that allow all orbital rotations (ρ_{frz}-SCF and ρ_{sum}-SCF) than for ρ_{frz}-SCFMI, showing again the importance of the SCFMI orbital rotation constraint even past the equilibrium separation. This strengthens the claim that most of the difference between the frozen energy of P_{frz} and that of ρ_{sum}-SCF used in DEDA is due to what SCFMI-based EDA schemes would consider charge transfer.

Due to constant density CT, the computed frozen interaction is attractive by a separation of 1.55 Å for ρ_{sum}-SCF and by a separation of 1.70 Å for ρ_{frz}-SCF. On the other hand, by the P_{frz} and ρ_{frz}-SCFMI models, the frozen energy is repulsive until a separation of more than 2.20 Å is reached. The effect of constant density polarization (the energy difference between the P_{frz} and ρ_{frz}-SCFMI models) is a quite substantial 50 kJ/mol for the most compressed coordinate values. However this value is still small compared to the magnitude of both the frozen and non-frozen EDA contributions and thus has little effect on the qualitative interpretation of the interaction.

Inclusion of relaxation due to constant density polarization in the frozen energy (i.e. ρ_{frz}-SCFMI) is worthwhile in principle for generating quantitative results, with the caveat of the presence of energetic errors associated with inexact constraint satisfaction. The ρ_{frz}-SCF and ρ_{sum}-SCF methods on the other hand produce both quantitatively and qualitatively different results from P_{frz}, approximately halving the non-frozen contribution in the equilib-

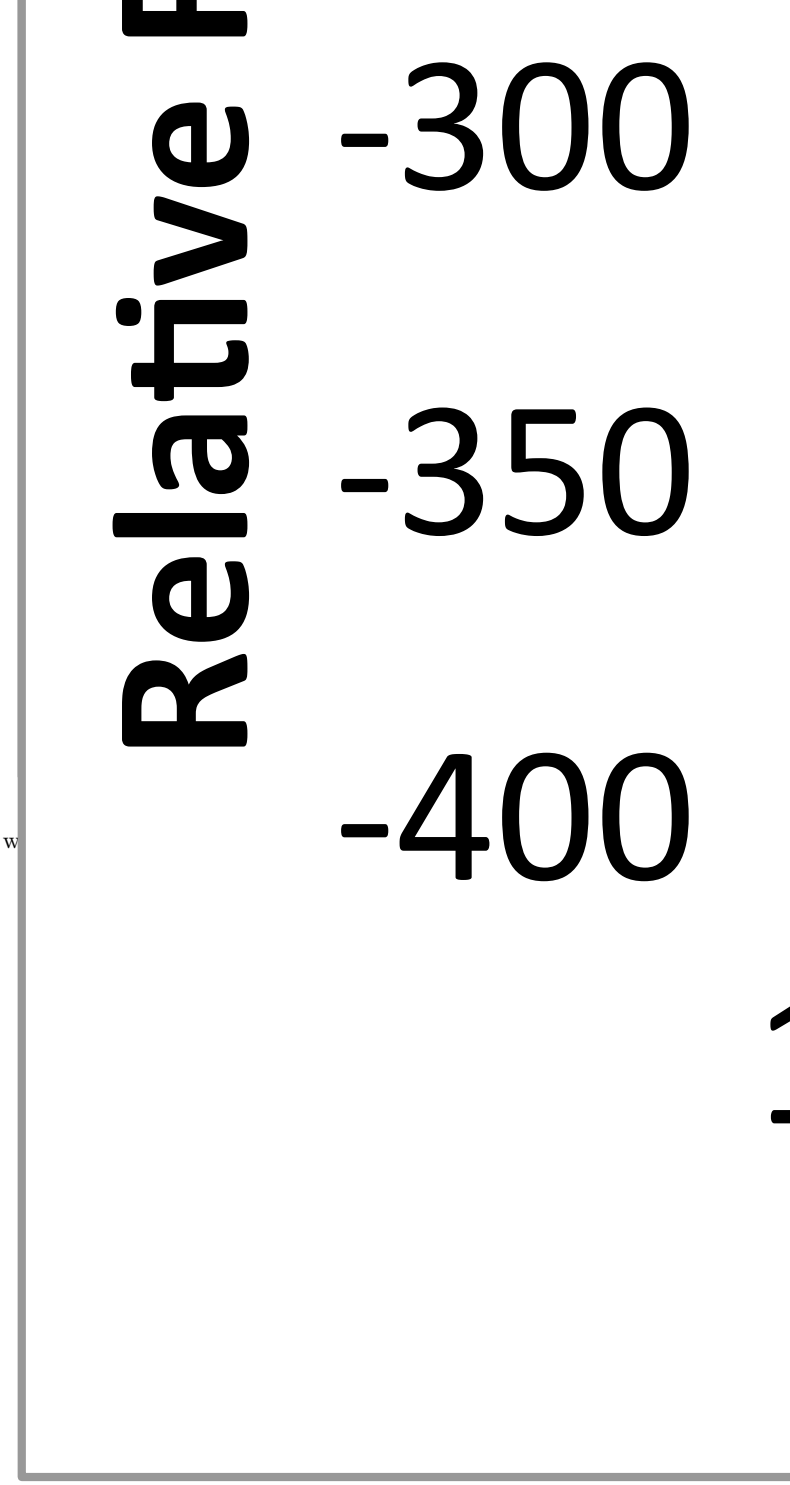

(b) Frozen energy deviations from that of the frozen orbital density matrix for several methods for NH_3-BH_3 at various interfragment (R_{N-B}) distances.

FIG. 7: Comparison of B3LYP/aug-cc-pVQZ frozen energies for the B3LYP/aug-cc-pVTZ relaxed R_{N-B} scan of NH_3-BH_3.

rium region. From the SCFMI-based EDA viewpoint, this change is unwanted, because it originates largely from constant density CT (i.e. the difference between ρ_{frz}-SCFMI and ρ_{frz}-SCF), which physically does not belong in the frozen energy.

D. Ethane Dissociation

Finally, we consider the frozen interaction energy of two methyl radicals, one of net α and one of net β spin as the first step in forming the covalent bond in the ethane molecule. Figure 8 shows both absolute (Figure 8a) and relative (Figure 8b) frozen energies computed for the four different models.

There is a dramatic difference between the frozen energy computed by schemes that include constant density CT degrees of freedom, ρ_{frz}-SCF and ρ_{sum}-SCF, and those that do not. The methods including the full SCF degrees of freedom during constant density optimization both suggest that bonding in ethane can be described almost entirely by the frozen interaction term with minimal contributions from non-frozen interactions, polarization and charge transfer. On the other hand, both the $\mathrm{P}_{\mathrm{frz}}$ and ρ_{frz}-SCFMI schemes suggest that the frozen contribution at this separation is destabilizing and that bonding is attained only after considering the collectively much larger non-frozen contributions.

We constrain the total spinless density instead of the separate spin densities in our constant 3-space density models, so it is possible for spin polarization to occur. To characterize the spin polarization, Figure 9 shows $\langle S^2 \rangle$ for each of the initial supersystem wavefunctions for ethane along the carbon-carbon bond breaking coordinate. Both the ρ_{frz}-SCF and ρ_{sum}-SCF initial wavefunctions show considerable spin depolarization (i.e. reduction of $\langle S^2 \rangle$ from its frozen orbital value) at short C-C distances. By contrast, the spin depolarization is much smaller in the ρ_{frz}-SCFMI model.

As ρ_{frz}-SCF and ρ_{sum}-SCF permit constant density CT, we conclude that spin recoupling at constant density is responsible for the spin depolarization in Figure 9 as well as the substantial energy lowering shown in Figure 8. For EDA purposes, it is essential that this constant density CT should be excluded from the frozen energy, as is the case in the ρ_{frz}-SCFMI and $\mathrm{P}_{\mathrm{frz}}$ models. Chemical bonding should not arise from the electrostatic, Pauli and dispersion interactions contained in a well-posed frozen energy. On the other hand, it is very interesting that density changes are a secondary contribution to the CC bond, relative to relaxation at constant density.

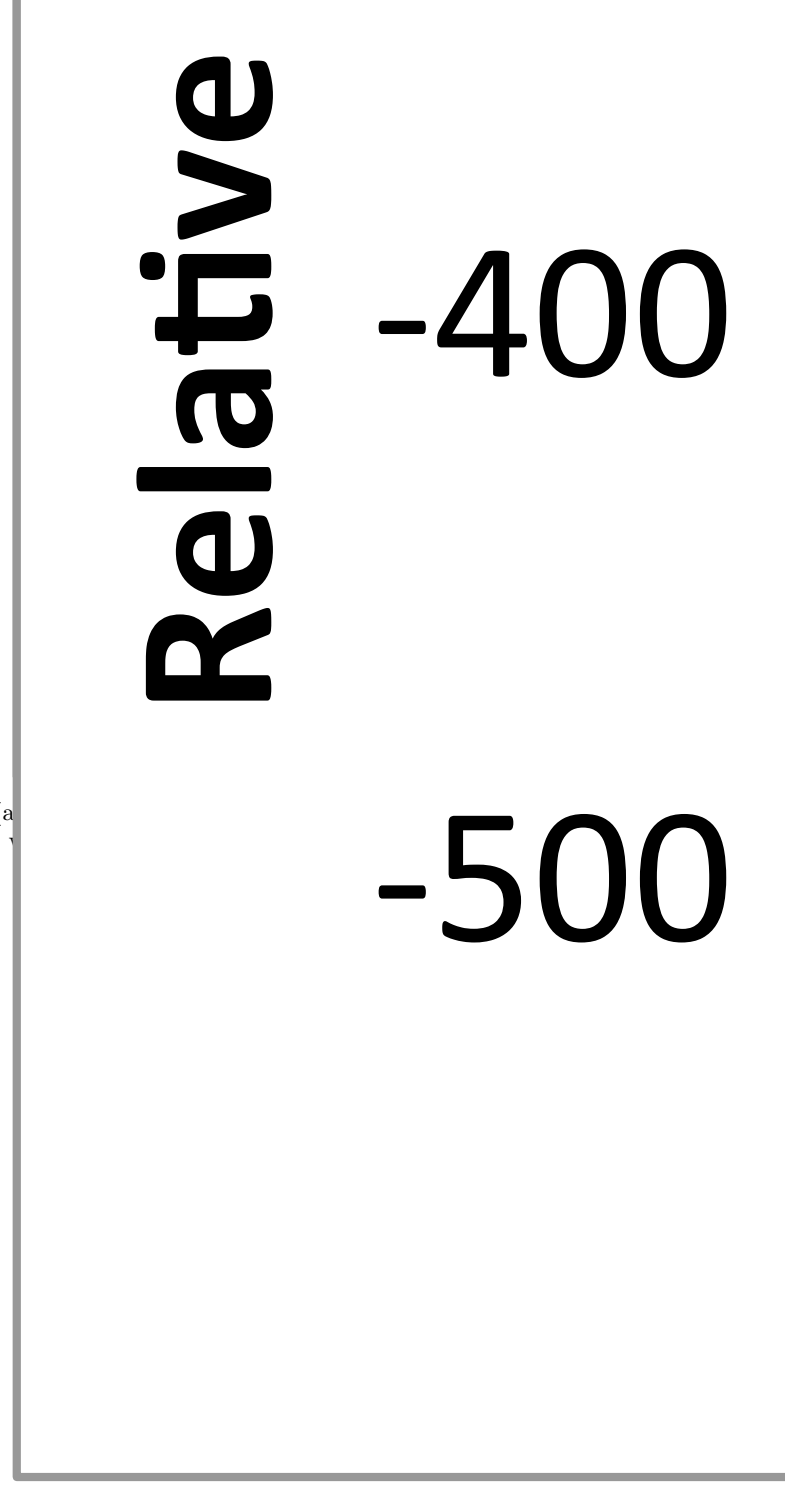

(b) Frozen energy by various methods relative to that of $\mathrm{P}_{\mathrm{frz}}$ for the dissociation of ethane.

FIG. 8: B3LYP/aug-cc-pVQZ frozen energy models for the rigidly $\mathrm{R}_{\mathrm{C-C}}$ dissociated net α and net β spin methyl fragments of B3LYP aug-cc-pVTZ optimized D_{3d} (staggered) ethane.

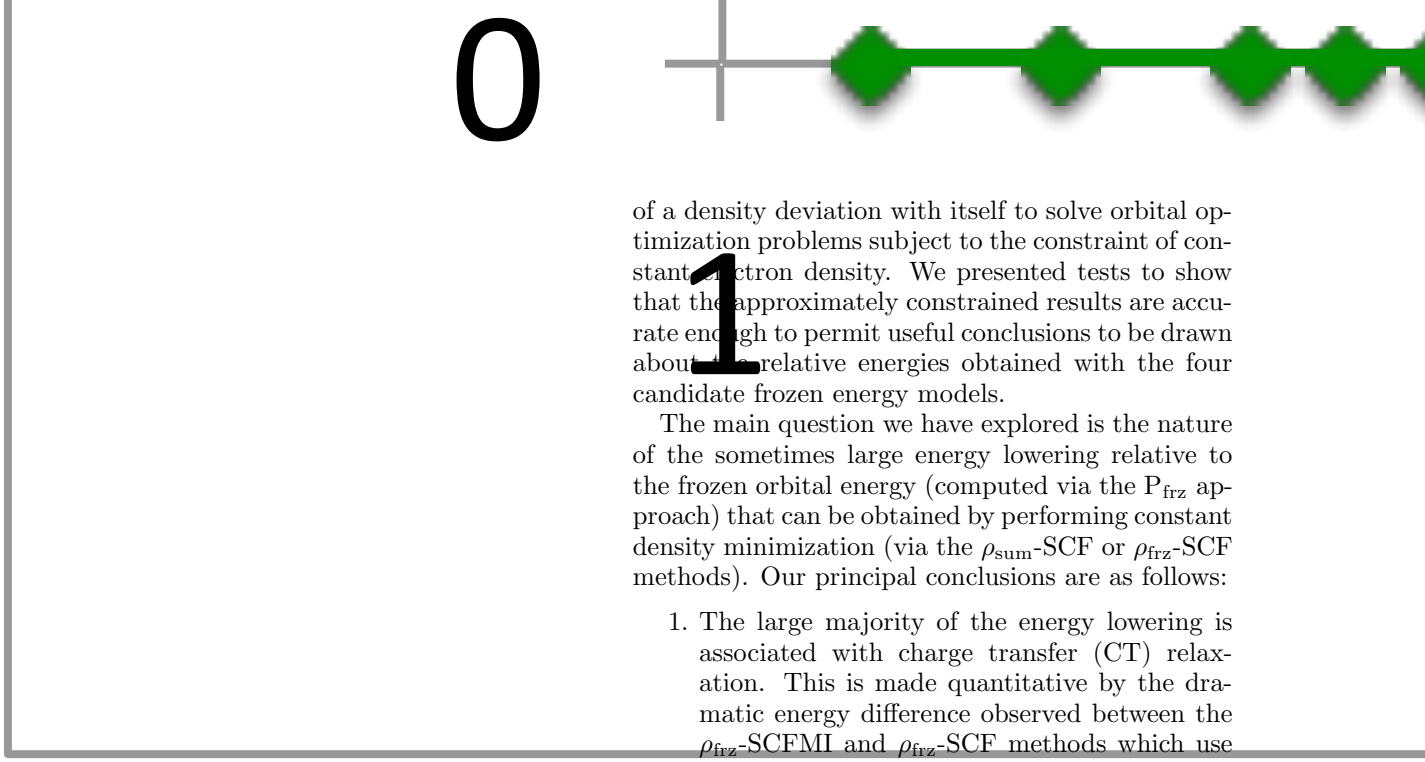

FIG. 9: B3LYP/aug-cc-pVQZ calculations of $\langle S^2 \rangle$ for initial supersystem wavefunctions of the rigidly dissociated B3LYP/aug-cc-pVTZ optimized D_{3d} staggered ethane molecule built from net alpha and net beta spin methyl fragments. Deviations from the $\langle S^2 \rangle$ value for P_{frz} signify orbital relaxation that changes the extent of spin polarization.

This is perhaps an encouraging conclusion from the perspective of reactive force fields.

The energy lowering associated with constant density polarization (i.e. $E_{\text{initial}}^{(\text{frz,SCFMI})}$-$E_{\text{initial}}^{\text{frz}}$), is about 100 kJ/mol at R_e, and it becomes more substantial for shorter carbon-carbon distances. As for ammonia borane, this changes the shape of the polarization contribution in SCFMI-based EDA schemes, particularly in the repulsive portion of the potential. It is thus in principle desirable to incorporate constant density relaxation using the ρ_{frz}-SCFMI initial wavefunction optimization, provided that the errors stemming from the violation of the constant $\rho(\mathbf{r})$ constraint are sufficiently small.

VI. CONCLUSIONS AND FUTURE WORK

In this work, we have addressed the question of how the initial supersystem wavefunction should be defined for energy decomposition analysis (EDA) of Kohn-Sham density functional theory calculations. The four different models defined in Table I were implemented and compared. To do so, we developed an algorithm based on the coulomb interaction of a density deviation with itself to solve orbital optimization problems subject to the constraint of constant electron density. We presented tests to show that the approximately constrained results are accurate enough to permit useful conclusions to be drawn about the relative energies obtained with the four candidate frozen energy models.

The main question we have explored is the nature of the sometimes large energy lowering relative to the frozen orbital energy (computed via the P_{frz} approach) that can be obtained by performing constant density minimization (via the ρ_{sum}-SCF or ρ_{frz}-SCF methods). Our principal conclusions are as follows:

1. The large majority of the energy lowering is associated with charge transfer (CT) relaxation. This is made quantitative by the dramatic energy difference observed between the ρ_{frz}-SCFMI and ρ_{frz}-SCF methods which use the same target density, but where CT relaxation is excluded by design in the former. Our view is that this constant ρ CT should not be a part of the frozen energy in an EDA composed of physically well-defined terms. It may be valuable for the development of force fields that have no explicit CT terms.

2. There is a much smaller effect from the choice between using ρ_{frz} or ρ_{sum} in the overlapping regime where they do differ. However, the latter does not necessarily admit feasible points in finite basis sets.

3. Including constant ρ polarization in the initial supersystem wavefunction, via the ρ_{frz}-SCFMI method, is an advance over the simple unrelaxed P_{frz} approach in an EDA, at least in principle. After all, intramonomer relaxation that does not change monomer charge distributions is not electrical polarization. However, our results show that this relaxation does not typically affect the qualitative interpretation of intermolecular interactions of weak to moderate strength. Our results therefore support the validity of existing EDAs which employ the frozen orbital model.

4. The merits of permitting orbital relaxation at constant density must be weighed against some illegitimate energy lowering introduced by imperfect constraint satisfaction. With our present methods, tests suggested this is not a serious problem when the relaxation is itself large, such as in the case of the SCF methods or in the case of the SCFMI approach in the strongly overlapping regime.

Regarding future work, it may be worthwhile, though it is clearly difficult, to further develop algorithms for more accurately enforcing constant density constraints. After all, the primary argument against the removal of constant density polarization from the initial supersystem wavefunction is the computational effort that must currently be expended for modest improvements.

VII. ACKNOWLEDGEMENTS

This work was supported by a grant (CHE-1363342) from the U.S. National Science Foundation.

[1]A. E. Reed, L. A. Curtiss, and F. Weinhold, Chem. Rev. **88**, 899 (1988).
[2]M. von Hopffgarten and G. Frenking, WIRES Comput. Mol. Sci. **2**, 43 (2012).
[3]Y. Mo, P. Bao, and J. Gao, Phys. Chem. Chem. Phys. **13**, 6760 (2011).
[4]M. J. S. Phipps, T. Fox, C. S. Tautermann, and C.-K. Skylaris, Chem. Soc. Rev. **44**, 3177 (2015).
[5]M. Rahm and R. Hoffmann, J. Am. Chem. Soc. **137**, 10282 (2015).
[6]P. O. Löwdin, Phys. Rev. **97**, 1490 (1955).
[7]W. A. Sokalski and M. R. Szczepan, Chem. Phys. Lett. **234**, 387 (1991).
[8]B. Jeziorski, R. Moszynski, and K. Szalewicz, Chem. Rev. **94**, 1887 (1994).
[9]S. J. Grabowski, W. A. Sokalski, and J. Leszczynski, J. Phys. Chem. A **109**, 4331 (2005).
[10]R. J. Azar and M. Head-Gordon, J. Chem. Phys. **136**, 024103 (2012).
[11]S. Iwata, P. Bandyopadhyay, and S. Xantheas, J. Phys. Chem. A **117**, 6641 (2013).
[12]J. Thirman and M. Head-Gordon, J. Chem. Phys. **143**, 084124 (2015).
[13]K. Kitaura and K. Morokuma, Int. J. Quantum Chem. **10**, 325 (1976).
[14]K. Morokuma, Acc. Chem. Res. **10**, 294 (1977).
[15]W. Chen and M. S. Gordon, J. Phys. Chem. **100**, 14316 (1996).
[16]D. G. Fedorov and K. Kitaura, J. Comput. Chem. **28**, 222 (2007).
[17]M. C. Green, D. G. Fedorov, K. Kitaura, J. S. Francisco, and L. V. Slipchenko, J. Chem. Phys. **138**, 074111 (2013).
[18]Y. Mochizuki, K. Fukuzawa, A. Kato, S. Tanaka, K. Kitaura, and T. Nakano, Chem. Phys. Lett. **410**, 247 (2005).
[19]S. Rybak, B. Jeziorski, and K. Szalewicz, J. Chem. Phys. **95**, 6576 (1991).
[20]A. Misquitta, B. Jeziorski, and K. Szalewicz, Phys. Rev. Lett. **91**, 033201 (2003).
[21]A. J. Misquitta, R. Podeszwa, B. Jeziorski, and K. Szalewicz, J. Chem. Phys. **123**, 214103 (2005).
[22]P. S. Zuchowski, R. Podeszwa, R. Moszyski, B. Jeziorski, and K. Szalewicz, J. Chem. Phys. **129**, 084101 (2008).
[23]F. M. Bickelhaupt and E. J. Baerends, Rev. Comput. Chem. **15**, 1 (2000).
[24]A. Krapp, F. M. Bickelhaupt, and G. Frenking, Chem. Eur. J. **12**, 9196 (2006).
[25]T. Ziegler and A. Rauk, Theor. Chim. Acta **46**, 1 (1977).
[26]T. Ziegler and A. Rauk, Inorg. Chem. **18**, 1558 (1979).
[27]M. P. Mitoraj, A. Michalak, and T. Ziegler, J. Chem. Theory Comput. **5**, 962 (2009).
[28]S. Ndambuki and T. Ziegler, Int. J. Quantum Chem. **113**, 753 (2013).
[29]P. Su and H. Li, J. Chem. Phys. **131**, 014102 (2009).
[30]P. Su, H. Liu, and W. Wu, J. Chem. Phys. **137**, 034111 (2012).
[31]P. Su, Z. Jiang, Z. Chen, and W. Wu, J. Phys. Chem. A **118**, 2531 (2014).
[32]P. . S. Bagus, K. Hermann, and C. W. J. Bauschlicher, J. Chem. Phys. **80**, 4378 (1984).
[33]W. J. Stevens and W. H. Fink, Chem. Phys. Lett. **139**, 15 (1987).
[34]P. Reinhardt, J.-P. Piquemal, and A. Savin, J. Chem. Theory Comput. **4**, 2020 (2008).
[35]P. De Silva and J. Korchowiec, J. Comput. Chem. **32**, 1054 (2011).
[36]M. Mandado and J. M. Hermida-Ramón, J. Chem. Theory Comput. **7**, 633 (2011).
[37]Y. Mo, J. Gao, and S. D. Peyerimhoff, J. Chem. Phys. **112**, 5530 (2000).
[38]Y. Mo, L. Song, and Y. Lin, J. Phys. Chem. A **111**, 8291 (2007).
[39]S. N. Steinmann, C. Corminboeuf, W. Wu, and Y. Mo, J. Phys. Chem. A **115**, 5467 (2011).
[40]R. Z. Khaliullin, M. Head-Gordon, and A. T. Bell, J. Chem. Phys. **124**, 204105 (2006).
[41]R. Z. Khaliullin, E. A. Cobar, R. C. Lochan, A. T. Bell, and M. Head-Gordon, J. Phys. Chem. A **111**, 8753 (2007).
[42]R. Z. Khaliullin, A. T. Bell, and M. Head-Gordon, J. Chem. Phys. **128**, 184112 (2008).
[43]P. R. Horn, E. J. Sundstrom, T. A. Baker, and M. Head-Gordon, J. Chem. Phys. **138**, 134119 (2013).
[44]A. Reed and F. Weinhold, J. Chem. Phys. **78**, 4066 (1983).
[45]E. D. Glendening and A. Streitwieser, J. Chem. Phys. **100**, 2900 (1994).
[46]G. K. Schenter and E. D. Glendening, J. Phys. Chem. **100**, 17152 (1996).
[47]E. D. Glendening, J. Phys. Chem. A **109**, 11936 (2005).
[48]Q. Wu, P. W. Ayers, and Y. Zhang, J. Chem. Phys. **131**, 164112 (2009).
[49]Q. Wu, J. Chem. Phys. **140**, 244109 (2014).
[50]J. Harriman, Phys. Rev. A **27**, 632 (1983).
[51]Z. Lu, N. Zhou, Q. Wu, and Y. Zhang, J. Chem. Theory Comput. **7**, 4038 (2011).
[52]P. R. Horn and M. Head-Gordon, J. Chem. Phys. **143** (2015).
[53]M. Head-Gordon, P. E. Maslen, and C. A. White, J. Chem. Phys. **108**, 616 (1998).
[54]R. McWeeny, Rev. Mod. Phys. **32**, 335 (1960).
[55]D. Bowler and M. Gillan, Comput. Phys. Commun. **120**, 95 (1999).
[56]H. Stoll, G. Wagenblast, and H. Preuss, Theor. Chim. Acta **57**, 169 (1980).
[57]G. F. Smits and C. Altona, Theor. Chim. Acta. **67**, 461 (1985).
[58]J. M. Cullen, Int. J. Quantum Chem. **40**, 193 (1991).
[59]E. Gianinetti, M. Raimondi, and E. Tornaghi, Int. J. Quantum Chem. **60**, 157 (1996).
[60]T. Nagata, O. Takahashi, K. Saito, and S. Iwata, J. Chem. Phys. **115**, 3553 (2001).
[61]R. J. Azar, P. R. Horn, E. J. Sundstrom, and M. Head-Gordon, J. Chem. Phys. **138**, 084102 (2013).

[62]A. Fornili, M. Sironi, and M. Raimondi, J. Mol. Struct: THEOCHEM **632**, 157 (2003).
[63]M. Sironi, A. Genoni, M. Civera, S. Pieraccini, and M. Ghitti, Theor. Chem. Acc. **117**, 685 (2007).
[64]T. Van Voorhis and M. Head-Gordon, Mol. Phys. **100**, 1713 (2002).
[65]P. Pulay, J. Comput. Chem. **3**, 556 (1982).
[66]J. Nocedal and S. J. Wright, *Numerical Optimization*, edited by P. Glynn and S. M. Robinson, Springer Series in Operations Research and Financial Engineering (Springer-Verlag, New York, 1999) pp. 224–227.
[67]A. Edelman, T. Arias, and S. Smith, SIAM J. Matrix Anal. Appl. **20**, 303 (1998).
[68]J. J. Moré and D. J. Thuente, ACM Trans. Math. Software **20**, 286 (1994).
[69]S. M. Sharada, D. Stück, E. J. Sundstrom, A. T. Bell, and M. Head-Gordon, Mol. Phys. **113**, 1802 (2015).
[70]R. Seeger and J. A. Pople, J. Chem. Phys. **66**, 3045 (1977).
[71]Y. Shao, L. F. Molnar, Y. Jung, J. Kussmann, C. Ochsenfeld, S. T. Brown, A. T. B. Gilbert, L. V. Slipchenko, S. V. Levchenko, D. P. O'Neill, R. a. DiStasio, R. C. Lochan, T. Wang, G. J. O. Beran, N. a. Besley, J. M. Herbert, C. Y. Lin, T. Van Voorhis, S. H. Chien, A. Sodt, R. P. Steele, V. a. Rassolov, P. E. Maslen, P. P. Korambath, R. D. Adamson, B. Austin, J. Baker, E. F. C. Byrd, H. Dachsel, R. J. Doerksen, A. Dreuw, B. D. Dunietz, A. D. Dutoi, T. R. Furlani, S. R. Gwaltney, A. Heyden, S. Hirata, C.-P. Hsu, G. Kedziora, R. Z. Khalliulin, P. Klunzinger, A. M. Lee, M. S. Lee, W. Liang, I. Lotan, N. Nair, B. Peters, E. I. Proynov, P. a. Pieniazek, Y. M. Rhee, J. Ritchie, E. Rosta, C. D. Sherrill, A. C. Simmonett, J. E. Subotnik, H. L. Woodcock, W. Zhang, A. T. Bell, A. K. Chakraborty, D. M. Chipman, F. J. Keil, A. Warshel, W. J. Hehre, H. F. Schaefer, J. Kong, A. I. Krylov, P. M. W. Gill, and M. Head-Gordon, Phys. Chem. Chem. Phys. **8**, 3172 (2006).
[72]Y. Shao, Z. Gan, E. Epifanovsky, A. T. Gilbert, M. Wormit, J. Kussmann, A. W. Lange, A. Behn, J. Deng, X. Feng, D. Ghosh, M. Goldey, P. R. Horn, L. D. Jacobson, I. Kaliman, R. Z. Khaliullin, T. Kuś, A. Landau, J. Liu, E. I. Proynov, Y. M. Rhee, R. M. Richard, M. a. Rohrdanz, R. P. Steele, E. J. Sundstrom, H. L. Woodcock, P. M. Zimmerman, D. Zuev, B. Albrecht, E. Alguire, B. Austin, G. J. O. Beran, Y. a. Bernard, E. Berquist, K. Brandhorst, K. B. Bravaya, S. T. Brown, D. Casanova, C.-M. Chang, Y. Chen, S. H. Chien, K. D. Closser, D. L. Crittenden, M. Diedenhofen, R. a. DiStasio, H. Do, A. D. Dutoi, R. G. Edgar, S. Fatehi, L. Fusti-Molnar, A. Ghysels, A. Golubeva-Zadorozhnaya, J. Gomes, M. W. Hanson-Heine, P. H. Harbach, A. W. Hauser, E. G. Hohenstein, Z. C. Holden, T.-C. Jagau, H. Ji, B. Kaduk, K. Khistyaev, J. Kim, J. Kim, R. a. King, P. Klunzinger, D. Kosenkov, T. Kowalczyk, C. M. Krauter, K. U. Lao, A. Laurent, K. V. Lawler, S. V. Levchenko, C. Y. Lin, F. Liu, E. Livshits, R. C. Lochan, A. Luenser, P. Manohar, S. F. Manzer, S.-P. Mao, N. Mardirossian, A. V. Marenich, S. a. Maurer, N. J. Mayhall, E. Neuscamman, C. M. Oana, R. Olivares-Amaya, D. P. ONeill, J. a. Parkhill, T. M. Perrine, R. Peverati, A. Prociuk, D. R. Rehn, E. Rosta, N. J. Russ, S. M. Sharada, S. Sharma, D. W. Small, A. Sodt, T. Stein, D. Stück, Y.-C. Su, A. J. Thom, T. Tsuchimochi, V. Vanovschi, L. Vogt, O. Vydrov, T. Wang, M. a. Watson, J. Wenzel, A. White, C. F. Williams, J. Yang, S. Yeganeh, S. R. Yost, Z.-Q. You, I. Y. Zhang, X. Zhang, Y. Zhao, B. R. Brooks, G. K. Chan, D. M. Chipman, C. J. Cramer, W. a. Goddard, M. S. Gordon, W. J. Hehre, A. Klamt, H. F. Schaefer, M. W. Schmidt, C. D. Sherrill, D. G. Truhlar, A. Warshel, X. Xu, A. Aspuru-Guzik, R. Baer, A. T. Bell, N. a. Besley, J.-D. Chai, A. Dreuw, B. D. Dunietz, T. R. Furlani, S. R. Gwaltney, C.-P. Hsu, Y. Jung, J. Kong, D. S. Lambrecht, W. Liang, C. Ochsenfeld, V. a. Rassolov, L. V. Slipchenko, J. E. Subotnik, T. Van Voorhis, J. M. Herbert, A. I. Krylov, P. M. Gill, and M. Head-Gordon, Mol. Phys. **113**, 184 (2015).
[73]T. H. J. Dunning, J. Chem. Phys. **90**, 1007 (1989).
[74]R. A. Kendall, T. H. J. Dunning, and R. J. Harrison, J. Chem. Phys. **96**, 6796 (1992).
[75]A. D. Becke, J. Chem. Phys. **98**, 5648 (1993).
[76]C. Lee, W. Yang, and R. G. Parr, Phys. Rev. B **37**, 785 (1988).
[77]A. Becke, Phys. Rev. A **38**, 3098 (1988).
[78]See supplemental material at [URL will be inserted by AIP] for plots that provide measures of the relatively small energy error due to incomplete constraint satisfaction for each of the examples studied in Section V.
[79]R. Z. Khaliullin, A. T. Bell, and M. Head-Gordon, Chem. Eur. J. **15**, 851 (2009).
[80]E. Ramos-Cordoba, D. Lambrecht, and M. Head-Gordon, Faraday Disc. **150**, 345 (2011).
[81]E. A. Cobar, P. R. Horn, R. G. Bergman, and M. Head-Gordon, Phys. Chem. Chem. Phys. **14**, 15328 (2012).